CHEMISTRY OF MATERIALS

Article

pubs.acs.org/cm

Core–Shell Structure of Monodisperse Poly(ethylene glycol)-Grafted Iron Oxide Nanoparticles Studied by Small-Angle X-ray Scattering

Tilman A. Grünewald,[†] Andrea Lassenberger,[‡] Peter D. J. van Oostrum,[‡] Harald Rennhofer,[†] Ronald Zirbs,[‡] Barbara Capone,[§] Iris Vonderhaid,[‡] Heinz Amenitsch,[⊥] Helga C. Lichtenegger,*[,†] and Erik Reimhult*[,‡]

[†]Department of Material Sciences and Process Engineering, University of Natural Resources and Life Sciences, Vienna, Peter-Jordan-Straße 82, A-1190 Vienna, Austria

[‡]Department of Nanobiotechnology, University of Natural Resources and Life Sciences, Vienna, Muthgasse 11, A-1190 Vienna, Austria

[§]Faculty of Physics, University of Vienna, Boltzmanngasse 5, A-1090 Vienna, Austria

[⊥]Institute for Inorganic Chemistry, Graz University of Technology, Stremayrgasse 9/V, A-8010 Graz, Austria

ABSTRACT: The promising applications of core–shell nanoparticles in the biological and medical field have been well investigated in recent years. One remaining challenge is the characterization of the structure of the hydrated polymer shell. Here we use small-angle X-ray scattering (SAXS) to investigate iron oxide core–poly(ethylene glycol) brush shell nanoparticles with extremely high polymer grafting density. It is shown that the shell density profile can be described by a scaling model that takes into account the locally very high grafting density near the core. A good fit to a constant density region followed by a star-polymer-like, monotonously decaying density profile is shown, which could help explain the unique colloidal properties of such densely grafted core–shell nanoparticles. SAXS experiments probing the thermally induced dehydration of the shell and the response to dilution confirmed that the observed features are associated with the brush and not attributed to structure factors from particle aggregates. We thereby demonstrate that the structure of monodisperse core–shell nanoparticles with dense solvated shells can be well studied with SAXS and that different density models can be distinguished from each other.

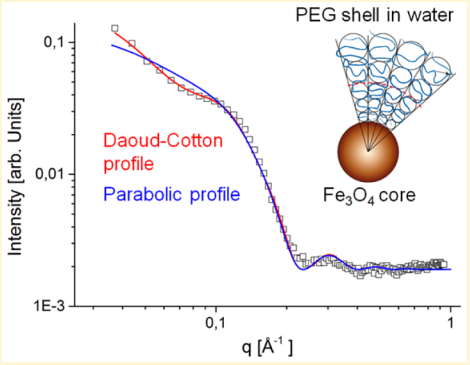

INTRODUCTION

Superparamagnetic Fe_3O_4 nanoparticles (NPs), with core diameters of 3–15 nm, are used in a rapidly expanding number of applications in the biomedical field; the most common include magnetic cell labeling,[1,2] hyperthermia,[3,4] drug delivery,[5] and as contrast agents for magnetic resonance imaging.[6−8] Rapid aggregation and precipitation of the iron oxide cores occur without a sterically stabilizing shell; a grafted polymer brush shell is the most stable and one of the most common surface modifications to enable dispersion of NPs in aqueous solutions containing biomolecules.

With recent improvements in the synthesis of NPs,[9] there has been a move toward more and more well-defined, core–shell particle architectures.[10] Monodisperse spherical iron oxide NPs can be synthesized with well-controlled magnetic and other physical properties;[11] these NPs should preferably be stabilized with an irreversibly anchored shell of linear, end-grafted polymer dispersants of sufficient thickness to ensure that the particle properties remain unaltered during application. This defined core–shell architecture enables the prediction of all colloidal properties and serves as a platform for further defining and designing physical, chemical, and biological interactions through the attachment of organic ligands. For example, the covalent grafting of dispersants to the core allows precise control over the hydrodynamic size, stability of the shell, and presentation of functional ligands in the shell; in contrast, NPs with dispersant shells formed by physisorption of high molecular weight dispersants are intrinsically not monodisperse and uniform nor can they ensure the presentation of attached ligands.[10] These differences critically determine the relative performance of the two types of NPs in a biological fluid.[12,13]

When stabilization is achieved by grafting of a polymer brush shell, the grafting density and the molecular weight of the grafted linear polymers will determine the density profile (hydration and thickness) of the shell. A thicker and denser shell has been shown to translate into higher colloidal stability under challenging environmental conditions including high concentrations of biomolecules.[14,15] It requires the irreversible grafting of polymers into a spherical brush by means of a high-

Received: April 27, 2015
Revised: June 17, 2015
Published: June 17, 2015

DOI: 10.1021/acs.chemmater.5b01488
Chem. Mater. 2015, 27, 4763−4771

affinity anchor group such as nitrocatechols for grafting to Fe_3O_4 NPs.[10,15]

A major challenge has been to achieve a dense grafting of dispersants also onto monodisperse cores since such cores are already coated with a high-affinity ligand of, for example, oleic acid after synthesis;[9] this ligand is difficult to replace with another dispersant at high density.[14,16] We recently introduced a new grafting method based on a two-step approach that creates NPs with complete ligand replacement and unsurpassed grafting density of poly(ethylene glycol) (PEG) dispersant.[14] NDA is used to replace oleic acid ligands and to provide an irreversibly bound anchor for the grafting of the PEG dispersant from a high-density melt of the polymer. The resulting core−shell iron oxide NPs have grafting densities approaching those limited by the footprint of the anchor molecule, and they display unique stabilities when dried, precipitated, heated, or exposed to high concentrations of proteins.[14] Since these properties are related to the density profile of the sterically/osmotically stabilizing spherical brush shell, an investigation of that structure is of highest interest for further optimization and functionalization of the shell. Previous theoretical and simulation works suggest that for very high grafting densities, a spherical brush will assume the segment density profile of a star polymer, which deviates strongly from a purely parabolic or Gaussian-type profile.[17,18] Our use of extremely monodisperse cores facilitates the interpretation of signals derived from the shell by minimizing signal smearing from size polydispersity. Thus, our newly developed monodisperse and densely grafted core−shell NPs are a highly interesting target for investigation of solvated shell structures.

Small-angle scattering (SAS) is a useful tool to study the size and internal structure of organic and inorganic colloids in the size range of 1−100 nm. For complex systems, SAS is advantageous compared to other methods because it allows studying the material in various solvents and environments; it is possible to characterize changes on the nanometer scale in situ and in a mostly nondestructive manner. SAS is therefore particularly valuable for studying the behavior of solid NPs with a polymer shell in biologically relevant solutions, where the solvent type and interaction with the polymer are known to strongly influence the conformation of the polymer shell.

One fundamental prerequisite for the use of scattering methods on particles in solution is the existence of a sufficiently high contrast in scattering length density between the solvent and the objects under investigation. The elemental composition of polymer shell and solvent is often similar, leading to a low contrast especially for strongly solvated shells such as PEG-brushes in water. The best contrast between polymer and water is provided by small-angle neutron scattering (SANS) in deuterated solvent. Hence, characterization of core−shell systems and in particular polymer micelles and star polymers has mainly been carried out by SANS.[19−21]

One major drawback of SANS is the limitation of experiments to a few, large facilities (spallation sources or reactors). In contrast to this, small-angle X-ray scattering (SAXS) can be performed on more common laboratory equipment or with extremely high brilliance at synchrotron facilities.[22] SAXS derives the signal from the electron density contrast between the different sample constituents. It was successfully used to characterize polymer micelles[23,24] and to characterize the interaction between different particles.[25−27] By comparing SAXS results with those from other methods such as transmission electron microscopy (TEM), dynamic light scattering (DLS), X-ray diffraction (XRD), or nitrogen sorption (BET) a very good agreement has been found in terms of size and polydispersity of a variety of NP and nanoporous systems especially between TEM and SAXS results for solid cores.[28,29]

SAXS analysis of the structure of inorganic core−solvated polymeric shell systems has been limited by the electron density contrast achievable between the core, the shell, and the surrounding solvent. In particular, the contrast between a highly hydrated polymer shell and water is low. A successful SAXS study was done, for example, on polystyrene chains on silica NPs dispersed in tetrahydrofuran[30] and in H_2O[31] to indirectly characterize the shell by means of analyzing the particle−particle interaction. The interaction of iron oxide NPs with hydrated PEG shells with respect to cluster formation was investigated on the basis of analysis of the interparticle distance and aggregation behavior of the solid cores (structure factor).[25−27] However, because of the low grafting density of the polymer, and consequently the low shell-to-solvent contrast, the shell was not visible enough to study its morphology (form factor) directly.[32]

We present the first investigation of the shell density profile of a highly solvated polymer brush shell grafted to an inorganic particle by SAXS. In this work, we demonstrate that the uniquely high polymer grafting densities that give these core−shell iron oxide NPs their unique colloidal properties also make the characterization of the associated density profiles possible by increasing the scattering length density contrast. We thereby also verify that approaching the theoretical limit for the grafting density of a spherical brush on NPs leads to a density profile best described by a star-polymer-like decay rather than the conventionally used parabolic or Gaussian-type profiles that oversimplify the internal structure of the core−shell particle.

EXPERIMENTAL SECTION

Chemicals Used for the Synthesis. All chemicals were reactant grade and used without further purification. Iron(0)pentacarbonyl ($Fe(CO)_5$, 99.99%), oleic acid ($CH_3(CH_2)_7CH{=}CH(CH_2)_7COOH$, ≥93%), dioctyl ether ($[CH_3(CH_2)_7]_2O$, >99%), PEG O-[2-(6-oxocaproylamino)ethyl]-O′-methylpolyethylene glycol (Mw 5000), dopamine hydrochloride ($(HO)_2C_6H_3CH_2CH_2NH_2{\cdot}HCl$), sulfuric acid H_2SO_4 (95−98%), sodium nitrite $NaNO_2$ (≥99%), Sephadex G75 (superfine), sodium chloride NaCl (≥99%), potassium sulfate K_2SO_4 (≥99%), and 3-(N-morpholino)propanesulfonic acid MOPS (≥99.5%) were purchased from Sigma-Aldrich, and ethanol C_2H_5OH (>96%) and dimethylformamide (DMF) (>99.9%) were obtained from Carl Roth. Purified Milli-Q (MQ) water was used for all experiments.

Core Synthesis. Superparamagnetic oleic acid stabilized NPs were synthesized by thermal decomposition of an iron precursor (iron(0)-pentacarbonyl) according to a slightly modified heat-up procedure[33] and described previously.[14] After magnetic separation and reprecipitation (two times) from toluene with ethanol (EtOH), the purified NPs were collected for further processing.

Nitrodopamine Priming by Ligand Exchange. Nitrodopamine (NDA) was used as anchor to prime the particles for grafting of aldehyde-poly(ethylene glycol) (ALD-PEG), as previously described.[14] NDA was chosen as primer and dispersant anchor because of its demonstrated nondestructive and irreversible binding to Fe_3O_4 NP surfaces.[15] NDA was synthesized following a modified method published earlier.[34] Ligand exchange of oleic acid against NDA was performed in DMF at room temperature for 16 h. After three-fold precipitation with EtOH and centrifugation (5000 rpm/5 min), the fully NDA-coated NPs were dried under an N_2 stream.

Melt Grafting. The grafting of ALD-PEG (5 kDa) to the NDA was performed as previously described.[14] Briefly, the iron oxide NDA-coated NPs were mixed under a continuous stream of N_2 in an excess

DOI: 10.1021/acs.chemmater.5b01488
Chem. Mater. 2015, 27, 4763−4771

of molten ALD-PEG in a glass vial and held at 100 °C for 2 h. After the reaction was completed, the mixture was cooled down to room temperature, and the particles were redispersed in MQ water and sonicated for 1 h.

Purification and Characterization of PEG-Grafted NPs. The NPs were gel-filtrated through a hand-packed 25 cm/2.5 cm Sephadex G75 column in pure water using just hydrostatic pressure to ensure removal of unbound excess ligands. The eluate was split into fractions, which were analyzed in terms of grafting density. The fractions with a grafting density of 3.5 chains/nm^2 as determined by TGA, displaying the highest colloidal stability,[14] were selected for all further experiments.

TEM Acquisition and Image Analysis. A small amount of product was dissolved in water (PEG-grafted NPs) or toluene (as-synthesized NPs) and dropped onto a TEM-grid (3.05 mm HR-TEM-grid, copper 300 mesh, carbon film). TEM images were obtained using a FEI Tecnai G2 200 kV transmission electron microscope at 200 kV. Core diameters were evaluated using the Pebbles software package[35] with a local intensity fitting algorithm. For this analysis, about 1000 particles were sampled by Pebbles.

TGA and Grafting Density. Samples of 1−3 mg each were weighed in 70 μL Alumina-cups and measured on a Mettler-Toledo TGA/DSC 1. The samples were measured under constant flow of synthetic air (80 mL/min) plus 20 mL/min nitrogen stream as protection gas for the balance at a heating rate of 10 K/min. Analysis was performed using the Mettler-Toledo software (simple step-function from 150 to 500 °C). The total organic content was determined from the mass loss occurring up to 500 °C, above which the Fe_3O_4 oxidizes. The total organic content was then used to calculate the grafting density based on the core diameter established by TEM (and confirmed by SAXS) and the known molecular weights of NDA and PEG.

Sample Preparation and SAXS Measurements. As-synthesized Fe_3O_4 NPs were prepared as a dry powder between two layers of Scotch tape and measured for 60 s.

The purified PEG-grafted NPs were diluted in MQ water to concentrations of 5, 1, and 0.5 mg/mL. Measurements were performed at room temperature.

The cloud point buffer measurements were performed on PEG-grafted NPs dispersed in MOPS buffer (0.5 M NaCl, 0.5 M K_2SO_4, and 0.08 M MOPS) at a concentration of 5.43 mg/mL. Measurements were performed in a temperature range from 20−50 °C with a heating and cooling rate of 1 K/min.

All solutions were loaded in type 0500 glass capillaries (Hilgenberg, Germany) with nominal diameter of 1 mm and wall thickness of 10 μm. They were flame-sealed to rule out contamination and finished with a droplet of epoxy resin to avoid any evaporation during the course of measurement.

Measurements were carried out using a Rigaku S-Max 3000 SAXS system equipped with a copper-target micro focus X-ray tube MicroMax-002+ (45 kV, 0.88 mA) with an energy of 8.05 keV, collimated through three pinholes (400, 200, and 700 μm) to achieve a beam diameter at the sample position of 210 μm (fwhm) and a Triton 200 2D multi wire gas-filled X-ray detector (200 mm diameter of active area, spatial resolution 200 μm). Data were acquired in the q-range from 0.01−0.95 Å^{-1} with a measurement time of 28.800 s for each scattering pattern at vacuum conditions better than 10^{-2} mbar. In situ heating experiments were carried out at the Austrian SAXS beamline at Elettra synchrotron Trieste, Italy, with a fixed energy of 8.00 keV.[36] For this experiment, a Pilatus3 1 M detector (Dectris, Switzerland) was used, which gave access to a q-range from 0.01−0.65 Å^{-1}. Heating was carried out using custom-made heating stage with water circulation. Measurement time was 2 s per scattering pattern.

Subsequent data treatment included background correction based on the measured transmission and radial integration with the SaxsGui 2.8.03 software package. In cases of large deviation in the capillary dimensions (± 5%), the transmission was normalized with the absorption of water through the equivalent thickness. To that end, the outer diameter of the capillaries was measured using a light microscope (Leica DM 4000 M). No deviations of the wall thickness were observed, and therefore no correction was needed.

SAXS Data Fitting Model. A theoretical model of the shell morphology was developed based on a mean field statistical approach to star polymers established by Daoud and Cotton[37] and was applied successfully to different core−shell[38] and micellar star polymer structures.[20] Following this approach, the spherical brush grafted to the NP core is represented by a sequence of concentric, close-packed blobs. Within every blob, chains behave as if they were free, hence following the free chain scaling laws. The local monomer concentration can be computed as a function of the radial distance r. The polymer shell around the grafted magnetite cores can be described as a star polymer with f branches (the number of grafted chains), each of which consists of N monomer units of lengths l, where l is taken to be half the Kuhn length. The Kuhn length depends on the monomer size, the flexibility of the chain, and the solvent quality; for PEG in water, it has been demonstrated that the PEG monomer length corresponds to half the Kuhn length, l.[39,40]

Because of the spherical symmetry of the system, the polymer brush covering the core is represented as a sequence of concentric blobs of radius $\xi(r)$, where r is the distance from the center of the particle. From geometrical considerations, it follows that the radius $\xi(r)$ of the close-packed blobs scales as

$$\xi(r) \approx rf^{1/2} \tag{1}$$

According to the Daoud−Cotton model, it is possible to distinguish three regions. A graphical representation of the partitioning of the shell into regions with different scaling behaviors is given in Figure 1.

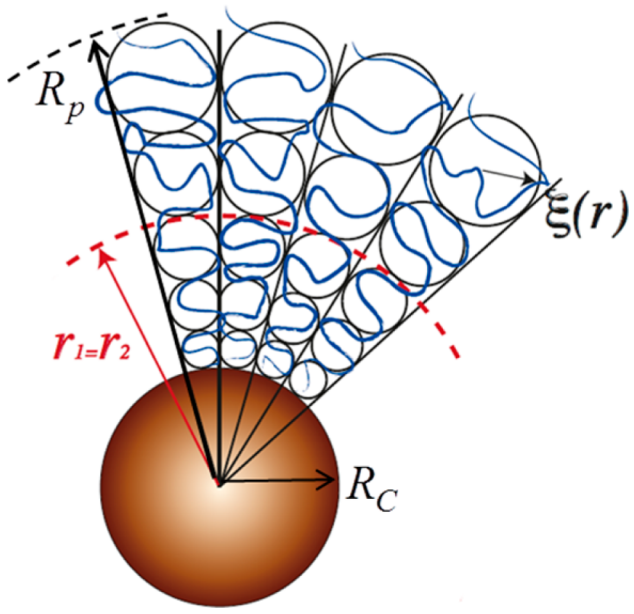

Figure 1. Representation of the Daoud−Cotton blob model for a spherical brush grafted to a solid core. $\xi(r)$ is the radius of an individual blob. The transition radius between melt-like (constant monomer concentration) and unswollen behavior is r_1. In the case of PEG, which has a negligible unswollen region, r_1 coincides with the transition radius between the unswollen and swollen regions, which is indicated by r_2. R_C is the radius of the iron oxide core, R_p the radius of the full particle.

The first region $r < r_1 = lf^{1/2}$ is characterized by a constant density of monomers. In this region, the grafted chains are so closely packed that the density corresponds closely to that of the pure polymer in a melt rather than that of a solvated state. Provided the grafting density is high enough, it directly determines the monomer concentration in this region. Originally called core region, the term "melt region" is used in this paper to avoid confusion with the iron oxide cores used as the

DOI: 10.1021/acs.chemmater.5b01488
Chem. Mater. 2015, 27, 4763−4771

grafting surface and to emphasize that this density is reached through the melt-grafting approach. Note that r_1 only depends on the number of arms, f, grafted to the surface and the monomer length l (dependent on the Kuhn length). Since r_1 does not contain the excluded volume parameter, it is only negligibly affected by factors such as temperature, molecular weight of the dispersant, or ion concentration compared to the outer part of the shell.

The region $r_1 < r < r_2$ is termed the "unswollen" region. Here, the behavior of the polymer is ideal even over distances longer than the blob radius $\xi(r)$. The polymer is solvated, and the volume it occupies is influenced by the solvent quality through the excluded volume parameter $\bar{\nu}$,[41] a measure of the interaction volume per monomer.

The "swollen" region starts at distance r_2 given by

$$r_2 = l\bar{\nu}f^{1/2} \tag{2}$$

In contrast to r_1, r_2 is also influenced by the excluded volume parameter and therefore solvent quality, which can be affected by factors such as ionic strength or temperature.

Since the excluded volume parameter $\bar{\nu}$ is one for PEG in water,[42] $r_1 = r_2$ and the unswollen region vanishes. For distances $r > r_2$, the polymer is self-avoiding at distances smaller than the blob radius $\xi(r)$. For self-avoiding polymer statistics, the monomer concentration scales with the radius as

$$c(r) \approx f^{2/3}\left(\frac{r}{l}\right)^{-4/3} l^{-3}\bar{\nu}^{-1/3} \tag{3}$$

The monomer concentration will thus follow the usual star polymer $r^{-4/3}$ decay.[37,41]

In this paper, we assume that the star polymer behavior will be essentially unchanged if the center of the star polymer is replaced by a solid core.

Eq 4 summarizes the concentration of monomers for the entire shell of a densely grafted NP with a PEG shell:

$$c(r)\begin{cases} = const, & \text{for } r < r_1 = r_2 \text{ "melt"} \\ \approx f^{2/3}\left(\frac{r}{l}\right)^{-4/3} l^{-3}\bar{\nu}^{-1/3}, & \text{for } r > r_1 = r_2 \text{ "swollen"} \end{cases} \tag{4}$$

The number of PEG chains attached to the core surface, f, is calculated from the grafting density ρ_{graft} (measured by TGA) and the core radius R_c (measured by TEM and SAXS on the bare cores):

$$f = \rho_{graft} 4\pi {R_c}^2 \tag{5}$$

The total number of monomers in the shell of a core−shell particle of total radius R_P has to equal the number of polymer chains times the number of monomers per chain N, a criterion which can be generally expressed as

$$Nf = 4\pi \int_{R_c}^{R_P} c(r) \times r^2 \, dr \tag{6}$$

with R_P the total core−shell particle radius. In our case, both the swollen region for $r > r_1 = r_2 = lf^{1/2}$, with a decaying monomer concentration, and the melt region for $r < r_1 = r_2 = lf^{1/2}$, where the monomer density equals $c(r)_{r=r1} = const$, contribute to the total number of monomers, which can be expressed as

$$Nf = 4\pi \int_{R_c}^{r_1} c(r)_{r=r_1} \times r^2 \, dr + 4\pi \int_{r_1}^{R_P} c(r)_{r=r_1}\left(\frac{r}{r_1}\right)^{-4/3} \times r^2 \, dr \tag{7}$$

By integration and rearranging, the monomer concentration in the constant density region $R_c < r < r_1 = r_2$ can be expressed as

$$c(r)_{r=r_1} = \frac{3}{4\pi}\frac{5Nf}{5({r_1}^3 - {R_c}^3) + 9{r_1}^{4/3}({R_P}^{5/3} - {r_1}^{5/3})} \tag{8}$$

The monomer concentration, $c(r)$ can then be used to calculate the electron density or scattering length density (SLD) profile plotted in Figure 2; the SLD of the shell consisting of monomers and water in SAXS is related to the ethylene glycol monomer concentration $c(r)$ by

$$SLD_{Shell}(r) = c(r) \times b_{coh,Mono} + \left(1 - \frac{c(r) \times m_{mol,Mono}}{N_A \times \rho_{Mono,melt}}\right) \times c_{H_2O} \times b_{coh,H_2O} \tag{9}$$

where $c(r)$ is the number density of the monomer molecules and c_{H2O} the number density of water molecules in pure water. $m_{mol,Mono}$ is the molar mass of the monomer, $\rho_{Mono,melt}$ the melt density of the monomer, and N_A the Avogadro number. $b_{coh,Mono}$ and $b_{coh,H2O}$ are the coherent scattering lengths of monomer and H_2O, respectively; the coherent scattering length is calculated from the atomic number Z of the constituting atoms and the classical electron radius as $b_{coh} = Z \times r_e$.

In practice, the SAXS signal depends on the scattering length density contrast of core and shell with respect to the solvent, and in particular on the concentration of monomer in the melt region. Therefore, we have defined a relative scattering length density of the melt region compared to that of the core. It is a measure of how much the shell contributes to the SAXS signal and therefore allows an estimate of the visibility of the shell:

$$\Delta SLD = \frac{SLD_{Shell}(r_1) - SLD_{H_2O}}{SLD_{Fe_3O4} - SLD_{H_2O}} \tag{10}$$

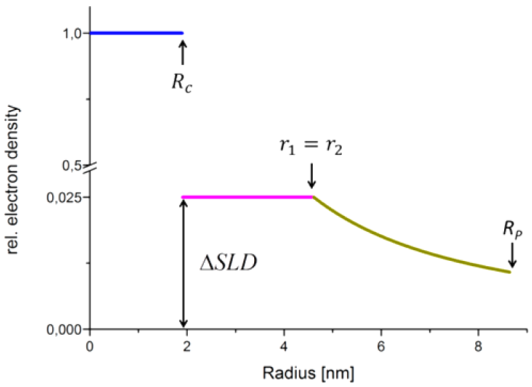

Figure 2. Relative radial electron density distribution in contrast to water and normalized with respect to the core (value of 1 in the core region, blue) is shown. It further consists of the constant density (melt) region (purple) and the $r^{-4/3}$ decay (swollen) region (green), as obtained from the monomer density distribution in eq 10. For reasons of visibility, the y-axis is truncated. The constant value ΔSLD denotes the relative scattering length density contrast of the shell in the melt region adjacent to the core, which is a measure of the maximum visibility of the shell.

The X-ray scattering is given by the Fourier transformation of the scattering length density variations encountered in a system, leading to the form factor $F(q)$ of a core−shell particle expressed as

$$F(q) = 4\pi \int_0^\infty SLD(r) r^2 \frac{\sin(qr)}{qr} \, dr \tag{11}$$

where q is the scattering vector:[43]

$$q = \frac{4\pi \sin(\theta)}{\lambda} \tag{12}$$

The combination of eqs 4, 10, and 11 leads to the fitted function:

$$I(q) = bg + amp \left| \int_0^\infty \psi(r) r^2 \frac{\sin(qr)}{qr} \, dr \right|^2 \tag{13}$$

DOI: 10.1021/acs.chemmater.5b01488
Chem. Mater. 2015, 27, 4763−4771

where bg is the constant background, amp the amplitude of the fit function, and $\psi(r)$ is given by

$$\psi(r) = = \begin{cases} 1 \text{ for } r < R_c & \text{“iron oxide core”} \\ \Delta SLD \text{ for } R_c < r < r_1 & \text{“PEG melt”} \\ \Delta SLD\left(\frac{r}{r_1}\right)^{-4/3} \text{ for } r_1 < r < R_P & \text{“PEG swollen”} \\ 0 \text{ for } r > R_P & \text{“solvent”} \end{cases} \quad (14)$$

The model (eq 13) was implemented in a Mathematica 9 script and fitted to the SAXS data in a q-range from 0.045−0.49 Å^{-1} using the free variables of total core−shell particle radius R_P and the scattering length density contrast of the constant density part of the shell ΔSLD. The value for the core radius was fixed to the values determined separately by the TEM measurements and shown to be consistent with SAXS measurements of the pure cores (see further). Fitting was carried out using a Levenberg−Marquardt algorithm weighted least-squares fit and evaluated by means of goodness-of-fit R^2 for the whole fit and the estimated standard errors for each fit parameter.

Once a constant density region is achieved through high enough grafting density, the ΔSLD is from a theoretical point of view a constant determined by the grafting density, Kuhn length, and the excluded volume of the monomers.

For the practical task of fitting the SAXS curves, however, it can be shown that the apparent value of ΔSLD is affected by the polydispersities in R_c, σ_{graft}, r_1, and R_P, which leads to smearing out of the signal and a lower apparent ΔSLD. Since it is practically impossible to determine each of these parameters individually, the approach of attributing their cumulative effect by leaving ΔSLD a free fit parameter was chosen. We emphasize that the polydispersity in each parameter is nevertheless unusually low due to the use of monodisperse cores and dispersants as well as the use of a grafting and purification method that results in an extremely high and uniform grafting density.[14]

RESULTS AND DISCUSSION

Core Size and Grafting Density. First, the iron oxide core size was determined by evaluating SAXS data and comparing the obtained hard sphere size to TEM data. Figure 3 shows the X-ray scattering intensity from dry cores coated with oleic acid (red squares) with the fit-function for the form and structure factors of hard spheres (monodisperse approximation) with Gaussian size distribution (black line). The diameter was determined to be 4.6 nm with a polydispersity of 7%.

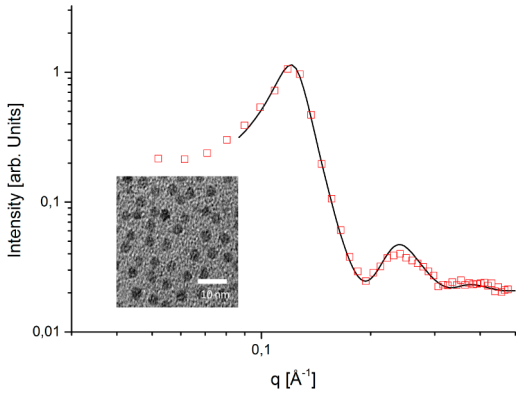

Figure 3. SAXS on as-synthesized, oleic acid coated cores as dry powder (red, squares) and the fitted function (black line). The inset shows a TEM micrograph of the particles, scalebar 10 nm.

Table 1 gives an overview of the results from the different methods to determine the core size. A manual analysis of the cores in the TEM images yields systematically smaller diameters than the other two methods. The discrepancy is attributed to the fact that the particle size is measured with the high contrast area taken as the particle. More advanced fitting of the TEM images using the software Pebbles uses the grayscale intensity to extrapolate the true extension of a spherical particle.[35] Thus, the TEM diameters evaluated using Pebbles are consistently larger than the manually measured diameters and in excellent agreement with the diameters determined by SAXS. This validates our use of TEM to determine the core diameters using Pebbles for the calculation of the grafting density of the shell. For the investigated particles, the total organic content was determined to be 91.1% [%w/w], which together with a PEG molecular weight of 5 kDa yields a grafting density of ∼3.5 chains/nm^2.

By using eq 5 and considering the cores grafted with PEG having a diameter of 3.7 nm, the minimum grafting density necessary to obtain a melt-like constant density region with a diameter ≥ 3.7 nm was found to be 0.55 chains/nm^2. This is far below the grafting density of 3.5 chains/nm^2 calculated from TGA and TEM data for the used particles. We therefore assumed the Daoud−Cotton model with a constant density region as the basis for fitting all acquired core−shell particle SAXS data.

Investigation of Particle−Particle Interaction (Structure Factor). The thickness of polymer shells grafted to NPs is highly dependent on the solvent, which is crucial to their functionality in biological environments. Measurements were carried out in MQ water and buffer solutions. Figure 4 shows a typical scattering curve from a core−shell particle in water and exhibits two distinct features; one in the high q-range from 0.23−0.42 Å^{-1}, which can be attributed to the core signal (cf. Figure 3), and a shoulder in the region of 0.12 Å^{-1}.

Similar shoulders have been reported in the literature. Various interpretations have been put forward ranging from particle−particle interactions (structure factor)[25] to dumbbell formation.[26,27] Therefore, a dilution series was carried out to ascertain that the shoulder could not be attributed to concentration-dependent particle−particle interaction (such as hard sphere interaction); a lower concentration will shift the peak position to smaller q if the shoulder results from particle−particle interactions.

The scattering curves in Figure 5 depict the scattering from core−shell particles at decreasing concentration. The shoulder is found at 0.12 Å^{-1} for all concentrations. The signal strength of all features decreases proportionally with decreasing concentration. We therefore conclude that the peak at 0.12 Å^{-1} is due to a permanent structural feature of the individual NPs (such as the shell) and cannot be attributed to a concentration-dependent structure factor. It should be noted that a shoulder due to a structure factor at 0.12 Å^{-1} would correspond to an interparticle distance of 5.2 nm and could therefore only be caused by NP cores in close proximity such as in dumbbells or other agglomerations of “naked” NPs. This option was investigated and its absence demonstrated by TEM and evidence from cloudpoint buffer experiments (see further below). We therefore fitted the SAXS signal with the core−shell electron density profile derived from the Daoud−Cotton theory.

Size and Scattering Contrast of the PEG Shell. Figure 6 displays model fits to the scattering curve in Figure 4. (blue).

DOI: 10.1021/acs.chemmater.5b01488
Chem. Mater. 2015, 27, 4763−4771

Table 1. Comparison of Core Radius and Polydispersity Measured by SAXS and TEM. Values Given for As-Synthesized Cores and the Cores in the Core−Shell NPs Originate from Different Batches.

sample	SAXS D [nm ± SD]	TEM D Pebbles [nm ± SD]/no. of particles	TEM D manual [nm ± SD]/no. of particles
As-synthesized Fe3O4 cores	4.6 ± 0.34	4.6 ± 0.30/1360	4.35 ± 0.25/252
Core−Shell particles, core	3.7 ± 0.42	3.8 ± 0.4/1209	3.4 ± 0.3/200

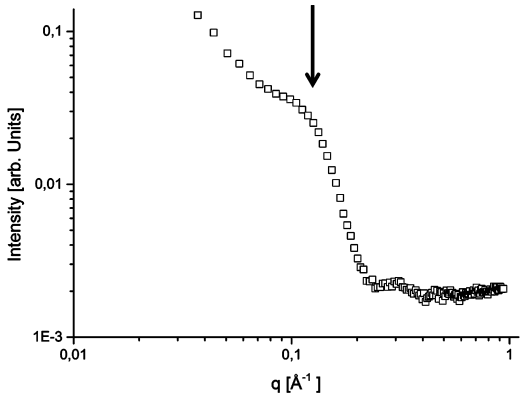

Figure 4. SAXS for 3.7 nm in diameter iron oxide core particles grafted with a PEG (5 kDa) shell of 3.5 chains/nm^2. The scattering from the cores is observed in the range from 0.23−0.42 Å^{-1} (cf. Figure 3). A distinct shoulder attributed to the shell is observed at 0.12 Å^{-1} (arrow). Particle concentration: 5 mg/mL.

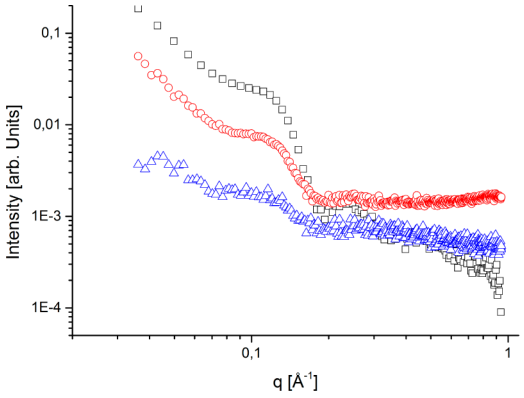

Figure 5. SAXS for 3.7 nm in diameter iron oxide core particles grafted with a PEG (5 kDa) shell of 3.5 chains/nm^2 at different concentrations (black, 5 mg/mL; red, 1 mg/mL; and blue, 0.5 mg/mL). The shoulder is found at 0.12 Å^{-1} for all concentrations.

The fit of the Daoud−Cotton model (red) is consistent with a constant density of the core, a high constant density region of PEG close to the core, and a decrease of PEG density according to $r^{-4/3}$ in the outer part of the shell as predicted for star polymers in a good solvent. The radius of the whole particle is obtained as R_P = 8.2 nm from this fit.

The limit of the constant density region (r_1) was calculated to be 4.6 nm as derived from the Daoud−Cotton model and the measured grafting density (eq 2).

The measured grafting density, together with the fitted R_P, translates to a monomer density at the core of 1.18 × 10^{22} cm^{-3}, which is close to but lower than the monomer density of 1.55 × 10^{22} cm^{-3} calculated for a PEG melt (calculated from Sigma-Aldrich datasheet values).

The scattering length density of the PEG shell at the core follows from this as 1.02 × 10^{11} cm^{-2} according to eq 9. According to eq 10, this yields ΔSLD = 0.025 compared to ΔSLD = 0.033 for pure melt, assuming a scattering length

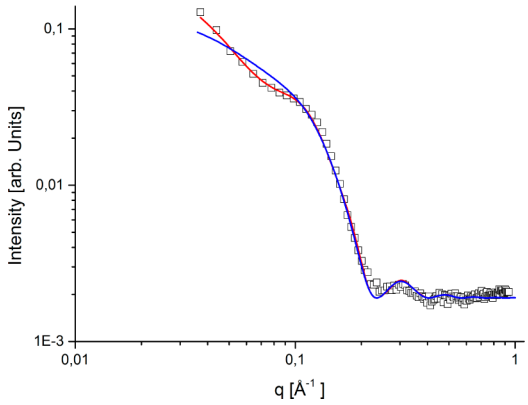

Figure 6. Representative fit of the Daoud−Cotton model for the core−shell particles in water (red line) and a parabolic "brush" density profile modeled to the obtained particle parameters (blue). The data set for the fit is shown as black squares.

density of 4.11 × 10^{11} cm^{-2} for the Fe_3O_4 cores and 9.43 × 10^{10} cm^{-2} for H_2O.

Note that curve fitting gave a value for the ΔSLD of 0.015 (Table 2). This is lower than the 0.025 calculated from the

Table 2. Fitted Values for Particle Radius and ΔSLD for Core−Shell NPs in Different Sample Environments

sample	R_P [nm]	ΔSLD
core−shell particles in MQ	8.2 ± 0.1	0.0143 ± 0.0007
cloud point 20 °C first step	8.8 ± 0.1	0.0119 ± 0.0003
cloud point 50 °C second step	7.4 ± 0.1	0.0248 ± 0.0001
cloud point 20 °C third step	8.6 ± 0.1	0.0195 ± 0.0004

fitted R_P by a factor of 0.6, which could partly be attributed to polydispersity of the shell. Furthermore, it should be noted that the R_P measured by SAXS relies on the contrast of the hydrated polymer shell with respect to water. It may not reflect the outermost radius of the shell that may fade out rather than end abruptly. The R_P measured by SAXS will represent a radius comprising the dense parts of the shell and the vast majority of, but possibly not all, monomers. This difference can also have contributed to the discrepancy between the fitted and calculated ΔSLD.

The core−shell particles exhibit a remarkable monodispersity evident also in the SAXS data both for core and shell features that justifies our approach. Substantial polydispersity would smear out the features to the point where they would be indistinguishable; the clearly visible features (two minima can be observed) show that the polydispersity is very low.

As comparison, the power law in eq 3 was replaced by a parabolic density profile, which is often used to approximate polymer brush density profiles; the corresponding scattering profile is depicted as the blue line in Figure 6. The values for R_P, *amp*, and *bg* were the same as those obtained by the fit of the Daoud−Cotton model; the ΔSLD was chosen to be the melt limit value of 0.033. It can be clearly seen that the parabolic

DOI: 10.1021/acs.chemmater.5b01488
Chem. Mater. 2015, 27, 4763−4771

density profile fails to describe the shoulder observed in the SAXS data, which was nicely captured by the Daoud−Cotton model.

Cloud Point Buffer Experiments. Shtykova et al. attributed a similar shoulder to what we observe at 0.12 $Å^{-1}$ to the formation of dumbbells for particles with lower polymer grafting density than in our samples.[27] Dumbbells were not observed by us in any TEM images; the cores of PEG-grafted NPs were always found well separated.

However, TEM is not acquired under solvated conditions, suffers from poor statistics, and might not show a representative sample. Therefore, to further test the dumbbell hypothesis on our samples, we investigated the influence of temperature on the shoulder peak in a so-called cloud point buffer that lowers the lower critical solution temperature (LCST) of PEG to ∼70 °C. If the shoulder is due to the PEG shell, temperatures approaching the LCST of the PEG should result in a decreasing shell thickness visible in the SAXS curve; dumbbells would not be affected by temperature changes.

A cyclic temperature program was chosen starting at 20 °C heating to 50 °C, then holding this temperature for 5 min and subsequently cooling to 20 °C. Heating and cooling was performed at 1 K/min and with 1 K temperature resolution.

The results of the temperature cycling show that the shoulder is indeed responsive to changing temperature (Figure 7) and that the change in shell size starts to take place already

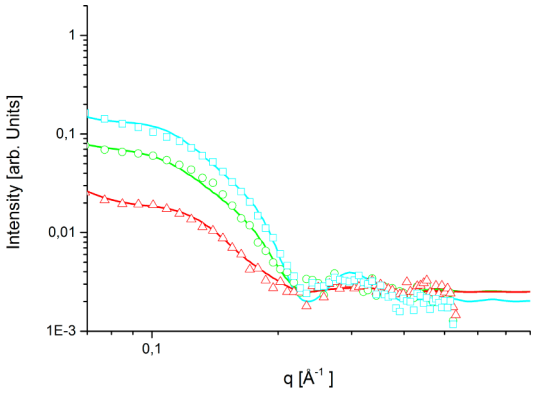

Figure 7. SAXS on iron oxide core−melt-grafted PEG shell particles in cloud point buffer for cyclic change of temperature. The temperature is cycled from 20 °C (green) to 50 °C (red) and subsequently cooled to 20 °C (cyan). Scattering data as symbols and Daoud−Cotton fits as solid lines.

at 35 °C (Figure 8). This means that the transition of the PEG brush to a less solvated state of lower thickness starts at a significantly lower temperature than what is observed for free PEG in the same buffer. We can only speculate to the reason for this, which merits a separate investigation; an explanation could be related to the much higher density of the PEG in the shell than for free solvated PEG and possibly a locally higher ion concentration due to specific ion interactions with the brush polymer. At a temperature of 50 °C, the shell is not fully collapsed and dehydrated.

At the initial 20 °C (green), the total particle radius including the shell has a fitted size of R_P = 8.8 nm, comparable to the size observed in water. Heating to 50 °C (red) shrinks the radius to $R_P \approx 7.5$ nm. The final cooling step to 20 °C (cyan) relaxes the particle radius to $R_P \approx 8.6$ nm, which within the margin of error is comparable to the initial particle radius. It is therefore once

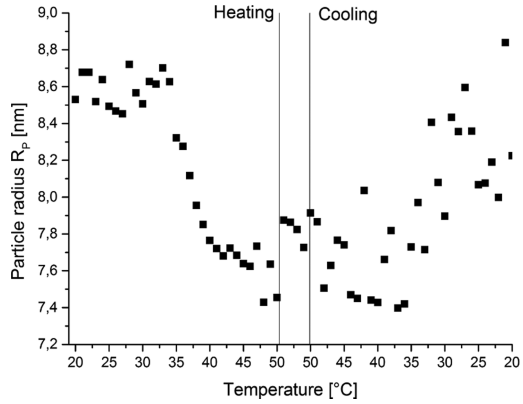

Figure 8. Total particle radius R_P iron oxide core−melt-grafted PEG shell particles in cloud point buffer in response to temperature changes.

more concluded that the shoulder is due to the PEG shell. This experiment shows not only the reversibility of the temperature-induced change in shell thickness, but also also shows that the shell always maintains a clearly defined size with low polydispersity, as otherwise the signal would vanish.

Some precipitation of the particles in the capillaries after temperature cycling was observed through the slight loss in scattering intensity. It cannot be ruled out that the precipitation in part is related to radiation damage or specific interactions introduced by the cloud point buffer. Previous investigations of colloidal stability at temperatures >70 °C of melt-grafted core−shell NPs in aqueous suspensions have shown remarkable stability without precipitation in water and excellent stability also at high temperature in PBS when investigated by turbidity measurements and by DLS.[14]

Table 2 shows the resulting fit values for the shell diameter and the Δ*SLD* for the PEG core−shell NPs in different sample environments; in all cases, the fits had $R^2 > 0.99$. The results for the particles in MQ water are fully consistent, as they indicate a monomer density lower than the limited imposed by a melt. The cloud point buffer temperature cycle measurements yield relatively different values for Δ*SLD* at the different temperatures. This is likely explained by the property of cloud point buffers to change the conformation and local ion concentration by specific interaction of the buffer salts with the polymer in the shell. A higher ion concentration within the brush than in the bulk due to specific interactions would increase Δ*SLD*. The Δ*SLD* parameter only governs the definition and shape of the shoulder and not its position. The observed change in the shoulder position can therefore be attributed to contraction and subsequent expansion of the shell during the temperature cycle.

CONCLUSIONS

We have characterized the core−shell structure of highly monodisperse and densely grafted iron oxide core−PEG-brush shell particles by SAXS. We have demonstrated the feasibility of using SAXS to characterize the size and swelling behavior of the PEG shell; this is in contrast to previous studies, in which much lower polymer grafting densities resulted in too low scattering length density contrast to resolve the shell. Great care was taken to rule out other contributions to the SAXS signal such as a structure peak from particle aggregation or dumbbells present from the synthesis by performing a dilution series and studying the temperature response of the size of the shell. Thereby, the

DOI: 10.1021/acs.chemmater.5b01488
Chem. Mater. 2015, 27, 4763−4771

appearance of a size-feature-specific to the shell could be proven.

The highly monodisperse NPs allowed the fitting of the shell density profile to a mean-field scaling model first derived by Daoud and Cotton for star polymers and adapted by us to densely grafted spherical brush core−shell NPs. This model quantitatively fitted the experimental data for all observable states of the shell including the temperature induced contraction of the shell in cloud point buffer. In contrast, a parabolic brush-type density profile could not reproduce the clear shoulder defined by the shell. These results support a constant monomer density region comparable to the density of the corresponding polymer melt closest to the core followed by a region of monotonously decreasing monomer density corresponding to that of a star polymer to describe the internal structure and unique colloidal properties of ultradensely grafted core−shell NPs.[14]

Our findings demonstrate that SAXS can be applied to structural studies of hybrid core−shell NP systems. This opens up new opportunities for the study of, for example, fast changes in core−shell NP structure. For such studies, SAXS has important advantages over competing techniques such as SANS as the experiments can be carried out with laboratory equipment or high brilliance synchrotron sources with very high time resolution.

The demonstrated existence of a "melt-like" polymer density in our core−shell particles close to the core could mean that aggregation or adsorption of such particles is only possible after destruction of the shell, leading to unique properties as emulsifiers, in hybrid materials and for biomedical applications.

AUTHOR INFORMATION

Corresponding Authors

*E-mail: erik.reimhult@boku.ac.at.

*E-mail: helga.lichtenegger@boku.ac.at.

Author Contributions

The manuscript was written through contributions of all authors. All authors have given approval to the final version of the manuscript.

Funding

The research leading to these results received funding from the European Research Council under the European Union's Seventh Framework Programme (FP/2007−2013)/ERC Grant Agreement No. 310034.

Notes

The authors declare no competing financial interest.

ACKNOWLEDGMENTS

The authors acknowledge the help and support of the Austrian SAXS beamline staff at Elettra. The VIBT Extremophile Center is acknowledged for access to TGA.

REFERENCES

(1) Lewin, M.; Carlesso, N.; Tung, C. H.; Tang, X. W.; Cory, D.; Scadden, D. T.; Weissleder, R. Tat peptide-derivatized magnetic nanoparticles allow in vivo tracking and recovery of progenitor cells. *Nat. Biotechnol.* **2000**, *18*, 410−414.

(2) Pittet, M. J.; Swirski, F. K.; Reynolds, F.; Josephson, L.; Weissleder, R. Labeling of immune cells for in vivo imaging using magnetofluorescent nanoparticles. *Nat. Protoc.* **2006**, *1*, 73−79.

(3) Halbreich, A.; Roger, J.; Pons, J. N.; Geldwerth, D.; Da Silva, M. F.; Roudier, M.; Bacri, J. C. Biomedical applications of maghemite ferrofluid. *Biochimie* **1998**, *80*, 379−390.

(4) Pankhurst, Q. A.; Thanh, N. K. T.; Jones, S. K.; Dobson, J. Progress in applications of magnetic nanoparticles in biomedicine. *J. Phys. D: Appl. Phys.* **2009**, *42*, 224001.

(5) Namdeo, M.; Saxena, S.; Tankhiwale, R.; Bajpai, M.; Mohan, Y. M.; Bajpai, S. K. Magnetic nanoparticles for drug delivery applications. *J. Nanosci. Nanotechnol.* **2008**, *8*, 3247−3271.

(6) Weissleder, R.; Hahn, P. F.; Stark, D. D.; Rummeny, E.; Saini, S.; Wittenberg, J.; Ferrucci, J. T. Mr imaging of splenic metastases-ferrite-enhanced detection in rats. *Am. J. Roentgenol.* **1987**, *149*, 723−726.

(7) Weissleder, R.; Elizondo, G.; Wittenberg, J.; Rabito, C. A.; Bengele, H. H.; Josephson, L. Ultrasmall superparamagnetic iron-oxide-characterization of a new class of contrast agents for Mr imaging. *Radiology* **1990**, *175*, 489−493.

(8) McCarthy, J. R.; Weissleder, R. Multifunctional magnetic nanoparticles for targeted imaging and therapy. *Adv. Drug Delivery Rev.* **2008**, *60*, 1241−1251.

(9) Park, J.; Joo, J.; Kwon, S. G.; Jang, Y.; Hyeon, T. Synthesis of monodisperse spherical nanocrystals. *Angew. Chem., Int. Ed.* **2007**, *46*, 4630−4660.

(10) Amstad, E.; Textor, M.; Reimhult, E. Stabilization and functionalization of iron oxide nanoparticles for biomedical applications. *Nanoscale* **2011**, *3*, 2819−2843.

(11) Park, S.-J.; Kim, S.; Lee, S.; Khim, Z. G.; Char, K.; Hyeon, T. Synthesis and magnetic studies of uniform iron nanorods and nanospheres. *J. Am. Chem. Soc.* **2000**, *122*, 8581−8582.

(12) Lu, A.-H.; Salabas, E. L.; Schueth, F. Magnetic nanoparticles: Synthesis, protection, functionalization, and application. *Angew. Chem., Int. Ed.* **2007**, *46*, 1222−1244.

(13) Jun, Y.-W.; Lee, J.-H.; Cheon, J. Chemical design of nanoparticle probes for high-performance magnetic resonance imaging. *Angew. Chem., Int. Ed.* **2008**, *47*, 5122−5135.

(14) Zirbs, R.; Lassenberger, A.; Vonderhaid, I.; Kurzhals, S.; Reimhult, E. Melt-grafting for the synthesis of core−shell nanoparticles with ultra-high dispersant density. *Nanoscale* **2015**, *7*, 11216−11225.

(15) Amstad, E.; Gillich, T.; Bilecka, I.; Textor, M.; Reimhult, E. Ultrastable iron oxide nanoparticle colloidal suspensions using dispersants with catechol-derived anchor groups. *Nano Lett.* **2009**, *9*, 4042−4048.

(16) Davis, K.; Qi, B.; Witmer, M.; Kitchens, C. L.; Powell, B. A.; Mefford, O. T. Quantitative measurement of ligand exchange on iron oxides via radio labeled oleic acid. *Langmuir* **2014**, *30*, 10918−10925.

(17) Lo Verso, F.; Yelash, L.; Egorov, S. A.; Binder, K. Effect of the solvent quality on the structural rearrangement of spherical brushes: Coarse-grained models. *Soft Matter* **2012**, *8*, 4185−4196.

(18) Lo Verso, F.; Egorov, S. A.; Milchev, A.; Binder, K. Spherical polymer brushes under good solvent conditions: Molecular dynamics results compared to density functional theory. *J. Chem. Phys.* **2010**, *133*, 184901.

(19) Pyckhout-Hintzen, W.; Allgaier, J.; Richter, D. Recent developments in polymer dynamics investigations of architecturally complex systems. *Eur. Polym. J.* **2011**, *47*, 474−485.

(20) Willner, L.; Jucknischke, O.; Richter, D.; Roovers, J.; Zhou, L. L.; Toporowski, P. M.; Fetters, L. J.; Huang, J. S.; Lin, M. Y.; Hadjichristidis, N. Structural investigations of star polymers in solution by small-angle neutron scattering. *Macromolecules* **1994**, *27*, 3821−3829.

(21) Dozier, W. D.; Huang, J. S.; Fetters, L. J. Colloidal nature of star polymer dilute and semidilute solutions. *Macromolecules* **1991**, *24*, 2810−2814.

(22) Lichtenegger, H. C.; Birkedal, H.; Casa, D. M.; Cross, J. O.; Heald, S. M.; Waite, J. H.; Stucky, G. D. Distribution and role of trace transition metals in *Glycera* worm jaws studied with synchrotron microbeam techniques. *Chem. Mater.* **2005**, *17*, 2927−2931.

(23) Rathgeber, S.; Pakula, T.; Urban, V. Structure of star-burst dendrimers: A comparison between small-angle X-ray scattering and computer simulation results. *J. Chem. Phys.* **2004**, *121*, 3840−3853.

(24) Furukawa, T.; Ishizu, K. Synthesis and viscoelastic behavior of multiarm star polyelectrolytes. *Macromolecules* **2005**, *38*, 2911−2917.

DOI: 10.1021/acs.chemmater.5b01488
Chem. Mater. 2015, 27, 4763−4771

(25) Fernandes, N. J.; Akbarzadeh, J.; Peterlik, H.; Giannelis, E. P. Synthesis and properties of highly dispersed ionic silica−poly(ethylene oxide) nanohybrids. *ACS Nano* **2013**, 1265−1271.
(26) Shtykova, E. V.; Huang, X.; Remmes, N.; Baxter, D.; Stein, B.; Dragena, B.; Svergun, D. I.; Bronstein, L. M. Structure and properties of iron oxide nanoparticles encapsulated by phospholipids with poly(ethylene glycol) tails. *J. Phys. Chem. C* **2007**, *111*, 18078−18086.
(27) Shtykova, E. V.; Malyutin, A.; Dyke, J.; Stein, B.; Konarev, P. V.; Dragena, B.; Svergun, D. I.; Bronstein, L. M. Hydrophilization of magnetic nanoparticles with modified alternativ copolymers. Part 2: Behavior in solution. *J. Phys. Chem. C* **2010**, *114*, 21908−21913.
(28) Pabisch, S.; Feichtenschlager, B.; Kickelbick, G.; Peterlik, H. Effect of interparticle interactions on size determination of zirconia and silica based systems—A comparison of SAXS, DLS, BET, XRD, and TEM. *Chem. Phys. Lett.* **2012**, *521*, 91−97.
(29) Darwish, M. S. A.; Peuker, U.; Kunz, U.; Turek, T. Bilayered polymer−magnetite core/shell particles: Synthesis and characterization. *J. Mater. Sci.* **2010**, *46*, 2123−2134.
(30) Kim, C. J.; Sondergeld, K.; Mazurowski, M.; Gallei, M.; Rehahn, M.; Spehr, T.; Frielinghaus, H.; Stühn, B. Synthesis and characterization of polystyrene chains on the surface of silica nanoparticles: Comparison of SANS, SAXS, and DLS results. *Colloid Polym. Sci.* **2013**, *291*, 2087−2099.
(31) Balmer, J. A.; Mykhaylyk, O. O.; Schmid, A.; Armes, S. P.; Fairclough, J. P.; Ryan, A. J. Characterization of polymer−silica nanocomposite particles with core−shell morphologies using Monte Carlo simulations and small-angle X-ray scattering. *Langmuir* **2011**, *27*, 8075−8089.
(32) Bronstein, L. M.; Shtykova, E. V.; Malyutin, A.; Dyke, J.; Gunn, E.; Gao, X.; Stein, B.; Konarev, P. V.; Dragena, B.; Svergun, D. I. Hydrophilization of magnetic nanoparticles with modified alternating copolymers. Part 1: The influence of the grafting. *J. Phys. Chem. C* **2010**, *114*, 21900−21907.
(33) Hyeon, T.; Lee, S. S.; Park, J.; Chung, Y.; Hyon, B. N. Synthesis of highly crystalline and monodisperse maghemite nanocrystallites without a size-selection process. *J. Am. Chem. Soc.* **2001**, *123*, 12798−12801.
(34) Yang, X.; Hong, H.; Grailer, J. J.; Rowland, I. J.; Javadi, A.; Hurley, S. A.; Xiao, Y.; Yang, Y.; Zhang, Y.; Nickles, R. J.; Cai, W.; Steeber, D. A.; Gong, S. cRGD-functionalized, DOX-conjugated, and (6)(4)Cu-labeled superparamagnetic iron oxide nanoparticles for targeted anticancer drug delivery and PET/MR imaging. *Biomaterials* **2011**, *32*, 4151−4160.
(35) Mondini, S.; Feretti, A. M.; Puglisi, A.; Ponti, A. PEBBLES and PEBBLEJUGGLER: Software for accurate, unbiased, and fast measurement and analysis of nanoparticle morphology from transmission electron microscopy (TEM) micrographs. *Nanoscale* **2012**, *4*, 5356−5372.
(36) Amenitsch, H.; Rappolt, M.; Kriechbaum, M.; Mio, H.; Laggner, P.; Bernstorff, S. First performance assessment of the small-angle X-ray scattering beamline at ELETTRA. *J. Synchrotron Radiat.* **1998**, *5*, 506−508.
(37) Daoud, M.; Cotton, J. P. Star-shaped polymers: A model for the conformation and its concentration dependence. *J. Phys. (Paris)* **1982**, *43*, 531−538.
(38) Vogiatzis, G. G.; Theodorou, D. N. Structure of polymer layers grafted to nanoparticles in silica−polystyrene nanocomposites. *Macromolecules* **2013**, *46*, 4670−4683.
(39) Hansen, P. L.; Cohen, J. A.; Podgornik, R.; Parsegian, V. A. Osmotic properties of poly(ethylene glycols): Quantitative features of brush and bulk scaling laws. *Biophys. J.* **2003**, *84*, 350−355.
(40) Kenworthy, A. K.; Hristova, K.; Needham, D.; McIntosh, T. J. Range and magnitude of the steric pressure between bilayers containing phospholipids with covalently attached poly(ethylene glycol). *Biophys. J.* **1995**, *68*, 1921−1936.
(41) Likos, C. N. Effective interactions in soft condensed matter physics. *Phys. Rep.* **2001**, *348*, 267−439.
(42) Dittmore, A.; McIntosh, D. B.; Halliday, S.; Saleh, O. A. Single-molecule elasticity measurements of the onset of excluded volume in poly(ethylene glycol). *Phys. Rev. Lett.* **2011**, *107*, 148301.
(43) Glatter, O.; Kratky, O. *Small-Angle X-ray Scattering*; Academic Press: London, 1982.

DOI: 10.1021/acs.chemmater.5b01488
Chem. Mater. 2015, 27, 4763−4771